

Oscillations and Bifurcation Structure of Reaction-Diffusion Model for Cell Polarity Formation

Masataka Kuwamura^{*}, Hirofumi Izuhara[†] and Shin-ichiro Ei[‡]

Abstract

We investigate the oscillatory dynamics and bifurcation structure of a reaction-diffusion system with bistable nonlinearity and mass conservation, which was proposed by [Otsuji et al, PLoS Comp. Biol. 3 (2007), e108]. The system is a useful model for understanding cell polarity formation. We show that this model exhibits four different spatiotemporal patterns including two types of oscillatory patterns, which can be regarded as cell polarity oscillations with the reversal and non-reversal of polarity, respectively. The trigger causing these patterns is a diffusion-driven (Turing-like) instability. Moreover, we investigate the effects of extracellular signals on the cell polarity oscillations.

Keywords: cell polarity oscillations, reaction-diffusion system, bistable nonlinearity

Mathematics subject classification: 35K57, 92B05

^{*}Graduate School of Human Development and Environment, Kobe University, Kobe 657-8501, Japan, email: kuwamura@main.h.kobe-u.ac.jp

[†]Faculty of Engineering, University of Miyazaki, 1-1 Gakuen Kibanadai-nishi, Miyazaki, 889-2192, Japan, email: izuhara@cc.miyazaki-u.ac.jp

[‡]Department of Mathematics, Hokkaido University, Sapporo 060-0810, Japan, email: Eichiro@math.sci.hokudai.ac.jp

1 Introduction

Reaction-diffusion systems with bistable nonlinearity are useful for understanding basic biological phenomena such as the population dynamics of competing species and propagating pulses on the nerve axon [18, 21]. As for cell polarization, which is a key process in cell division and differentiation, [15] proposed a reaction-diffusion model with bistable nonlinearity for understanding the wave-pinning phenomena: A transient and localized stimulus to an unpolarized cell is spatially amplified to result in a robust subdivision of the cell into two clearly defined regions, front and back. Although the bistability in their model, which is represented by a Hill function, may not explicitly correspond to concrete molecular networks, it is a simple (phenomenological) model and hence allows us to explain a mechanism referred to as the wave-pinning by a mathematical analysis. Moreover, [16] investigated the bifurcation structure of the model in [15].

The maintenance of cell polarity can be considered as a dynamic process. In fact, cells in a developing epithelial tissue alternately repeat the establishment and loss of polarity in a cell cycle-dependent manner. This repetition is known as a cell polarity oscillation [3], where the reversal of polarity does not occur in such a way that the cells in an epithelial tissue are organized into layers. Moreover, cell polarity oscillations are also observed in cell migration, which is the directed movement of a single cell or a group of cells in response to chemical and/or mechanical signals. For example, bacteria cells during rippling (accordion-like movements) [4, 25] and migrating melanoma cells derived from tumors [24] can reverse their polarity in an oscillatory fashion.

For understanding cell polarity oscillations, some mathematical models have been proposed. For example, [24] proposed an ODE system based on biomolecular dynamics at the front and back lamellipodia in a migration

cell to better understand their experimental results concerning the change of cell polarity in melanoma cells derived from tumors. [4] proposed an ODE system based on three proteins to understand cell polarity oscillations with the polarity reversal of bacteria cells during rippling (accordion-like movements) [25]. [12] proposed a delay reaction-diffusion equation with a nonlocal term for studying the effects of a delayed negative feedback on cell polarity oscillations with the aid of numerical simulations. Recently, [28] generalized the ODE system in [4], and proposed an ODE system that generates four different mechanisms for switching cell polarity, including a mechanism to generate the periodic reversal of polarity.

In this paper, we consider a reaction-diffusion model with bistable non-linearity proposed by [23], which exhibits dynamics similar to that of considerably realistic reaction-diffusion models based on concrete molecular species and networks concerning cell polarity formation [19, 23, 27]:

$$\begin{cases} \dot{u} &= d_1 u_{xx} + f(u, v) \\ \dot{v} &= d_2 v_{xx} - f(u, v) \end{cases} \quad (1.1)$$

with

$$f(u, v) = a_1(u + v)\{(\alpha u + v)(u + v) - a_2\} \quad (1.2)$$

and

$$\alpha = \frac{d_1}{d_2}, \quad (1.3)$$

where d_1, d_2, a_1 , and a_2 are positive constants. We consider that u and v correspond to chemicals in the membrane and cytosol of a cell, respectively. Since the diffusion in the cytosol is faster than that in the membrane, the diffusion coefficients d_1 and d_2 satisfy the condition

$$d_1 < d_2,$$

which implies $0 < \alpha < 1$. We note that u and v should be considered as deviations from the reference values of the concentrations of the chemicals because either u or v can be negative, even if the initial values of u and v are positive as seen in the next section. Moreover, by setting $a_2 \rightarrow a_2 - \varepsilon a_E(x)$ in (1.2), we obtain the perturbed system of (1.1), i.e.,

$$\begin{cases} \dot{u} &= d_1 u_{xx} + \{f(u, v) + \varepsilon g(x, u, v)\} \\ \dot{v} &= d_2 v_{xx} - \{f(u, v) + \varepsilon g(x, u, v)\} \end{cases} \quad (1.4)$$

with

$$g(x, u, v) = a_1(u + v)a_E(x), \quad (1.5)$$

where $a_E(x)$ is a smooth function that represents the waveform of an extracellular signal, and ε is a small positive parameter that controls the amplitude of the extracellular signal. We consider (1.1) and (1.4) on an interval $I = (-K/2, K/2)$ under the periodic boundary condition for sufficiently large K .

In general, a reaction-diffusion system (1.1) with a smooth function f is called a reaction-diffusion system with mass conservation because

$$\xi := \frac{1}{K} \int_0^K (u(x, 0) + v(x, 0)) dx \equiv \frac{1}{K} \int_0^K (u(x, t) + v(x, t)) dx \quad (1.6)$$

holds for any (smooth) solutions under the periodic or Neumann boundary conditions. For certain functions f and boundary conditions, some mathematical aspects of (1.1) have been studied elsewhere [1, 6, 8, 16, 17, 22], and one of the typical dynamics of (1.1) is summarized as follows: Solutions with initial values near a homogeneous equilibrium destabilized through the same mechanism as the Turing instability eventually approach a localized unimodal stationary pattern (see, Figure 2). This dynamics is interpreted as cell polarization, and the position of the peak of the localized unimodal pattern determines the direction of the polarity. As for the function f given

by (1.2), it was numerically shown in [23] that (1.1) has such dynamics under certain conditions. In addition, [23] performed a formal stability analysis for the final localized unimodal stationary pattern of (1.1), and numerically showed that a solution of (1.4) starting from the final pattern of (1.1) can translationally move to the maximum point of $a_E(x)$ when $a_E(x)$ is given by $a_E(x) = A \cos(2\pi x/K)$. This implies that cell polarity can be controlled by extracellular signals.

In contrast, using the normal form theory, it was shown in [22] that (1.1) can have a unimodal stationary pattern, which changes its stability due to a Hopf bifurcation when we vary d_1 as a bifurcation parameter. Consequently, (1.1) with (1.2) has a spatially nonhomogeneous limit cycle with small amplitude under certain conditions.

The purpose of this paper is to show that (1.1) with (1.2) exhibits four different spatiotemporal patterns including two types of oscillatory patterns, which can be regarded as cell polarity oscillations with the reversal and non-reversal of polarity, respectively. Our numerical simulations show that (1.1) with (1.2) has large amplitude limit cycles (see, Figure 3). These limit cycles exhibit an alternating repetition of unimodal and spatially homogeneous patterns, and hence can be interpreted as cell polarity oscillations. Moreover, using a numerical bifurcation analysis, we investigate the bifurcation structure of (1.1) with (1.2), which generates the limit cycles when we vary d_1 as a bifurcation parameter. The result suggests that d_1 and ξ defined by (1.6) play a key role in the switching cell polarity. Furthermore, when $a_E(x)$ is given by $a_E(x) = A \cos(2\pi x/K)$, we investigate the dynamics of (1.4) with (1.2) and (1.5). In particular, we numerically show that (1.4) with (1.2) and (1.5) has limit cycles exhibiting such an alternating repetition. To understand the controllability of cell polarity oscillations by extracellular signals,

we examine the position of the peak of the periodically appearing unimodal patterns.

The remainder of this paper is organized as follows. In Section 2, we describe the bistability of an ODE system obtained from (1.1) by dropping the diffusion terms. Our characterization of the bistability is different from that of [15, 16]. In Section 3, we investigate spatiotemporal patterns of the unperturbed system (1.1) with (1.2). We give a concrete expression of a localized unimodal stationary pattern of (1.1) with (1.2) for sufficiently large K . As a prominent feature, this model enables us to perform concrete calculations for a mathematical analysis. Moreover, we numerically show the formation process of the localized unimodal stationary pattern and the existence of limit cycles, which exhibit an alternating repetition of unimodal and spatially homogeneous patterns. Consequently, we see that (1.1) with (1.2) exhibits four different spatiotemporal patterns including two types of oscillatory patterns, which can be regarded as cell polarity oscillations with the reversal and non-reversal of polarity, respectively. In Section 4, using a numerical bifurcation analysis, we investigate the bifurcation structure of (1.1) with (1.2) when we vary d_1 as a bifurcation parameter. Our numerical bifurcation analysis shows that the limit cycles exhibiting the alternating repetition bifurcate from the localized unimodal stationary pattern through a Hopf bifurcation, and that the limit cycles become unstable through a period doubling bifurcation. These results support the results obtained by numerical simulations in Section 2, and show that the trigger causing the spatiotemporal patterns is a diffusion-driven (Turing-like) instability. In Section 5, we investigate the dynamics of spatiotemporal patterns in the perturbed system (1.4) with (1.2) and (1.5) when $a_E(x)$ is given by $a_E(x) = A \cos(2\pi x/K)$. We analytically derive the equation of motion for the translational movement of

the localized unimodal pattern, which gives a mathematical justification of the results in [23]. Moreover, we show that (1.4) with (1.2) and (1.5) has limit cycles exhibiting such an alternating repetition, and examine whether the position of the peak of the periodically appearing unimodal pattern can be determined by the maximum point of $a_E(x)$. These results are useful for understanding the effects of extracellular signals on cell polarity oscillations. Section 6 discusses the results of this study.

2 The dynamics of ODE system

In this section, we investigate the dynamics of an ODE system obtained from (1.1) by dropping the diffusion terms. Our characterization of the bistability of the ODE system is different from that of [15, 16].

We consider the dynamics of

$$\begin{cases} \dot{u} &= f(u, v) \\ \dot{v} &= -f(u, v) \end{cases} \quad (2.1)$$

with

$$f(u, v) = a_1(u + v)\{(\alpha u + v)(u + v) - a_2\}, \quad (2.2)$$

where $a_1 > 0$, $a_2 > 0$ and $0 < \alpha < 1$. It is easy to see that $f(u, v) = 0$, an equation for u with arbitrarily fixed v , has three roots $h_1(v) < -v < h_2(v)$, where

$$\lim_{v \rightarrow \infty} \left| h_1(v) + \frac{v}{\alpha} \right| = 0 \quad \text{and} \quad \lim_{v \rightarrow -\infty} |h_1(v) + v| = 0,$$

and

$$\lim_{v \rightarrow \infty} |h_2(v) + v| = 0 \quad \text{and} \quad \lim_{v \rightarrow -\infty} \left| h_2(v) + \frac{v}{\alpha} \right| = 0.$$

We note that any solution of (2.1) satisfies $u + v = \xi$ for some ξ , and that

$$\dot{u} = f(u, \xi - u) = -a_1\xi^2(1 - \alpha)u + a_1\xi^3 - a_1a_2\xi \quad (2.3)$$

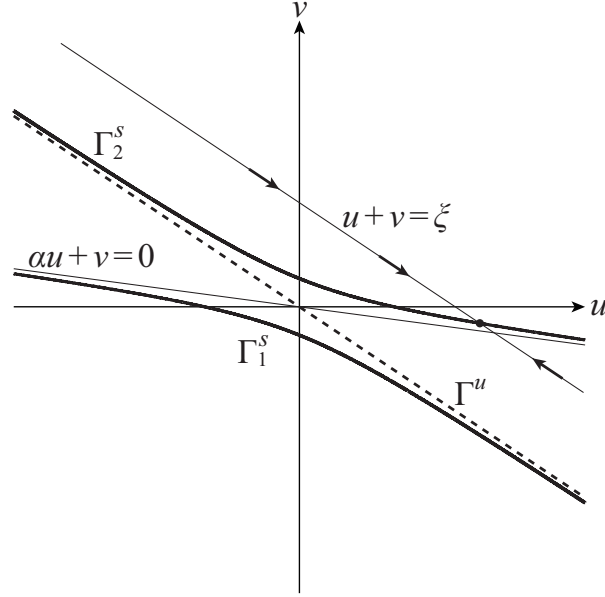


Figure 1: The dynamics of the ODE system (2.1) with (2.2).

has a unique stable equilibrium for $\xi \neq 0$ by $0 < \alpha < 1$. Hence, we see that (2.1) has a stable equilibrium

$$\left(\frac{\xi^2 - a_2}{(1 - \alpha)\xi}, \frac{a_2 - \alpha\xi^2}{(1 - \alpha)\xi} \right) \quad (2.4)$$

with $\xi \neq 0$, which corresponds to the stable equilibrium of (2.3) for $\xi \neq 0$. Therefore, we see that (2.1) has two families of stable equilibria $\Gamma_1^s = \{(h_1(v), v) \mid v \in \mathbf{R}\}$ and $\Gamma_2^s = \{(h_2(v), v) \mid v \in \mathbf{R}\}$, and a family of unstable equilibria $\Gamma^u = \{(-v, v) \mid v \in \mathbf{R}\}$. Thus, we can consider that (2.1) is bistable in the usual sense because it has two equivalent stable states Γ_1^s and Γ_2^s , and one unstable state Γ^u , which is a separatrix as seen in Figure 1. Moreover, we note that the dynamics of (2.1) does not qualitatively change when we vary $\alpha \in (0, 1)$.

Remark 2.1 Although we cannot apply a standard argument concerning the invariant region of reaction-diffusion systems [26], the phase plane in Figure 1 and numerical simulations suggest that $\{(u, v) \mid u + v > 0\}$ is an invariant region of the PDE (1.1) with (1.2) as well as the case of the ODE (2.1) with (2.2).

We note that for each fixed v , the ODE $\dot{u} = f(u, v)$ is monostable because it has two unstable equilibria $h_1(v)$ and $h_2(v)$, and one stable equilibrium $-v$. This is equivalent to a condition in which for each fixed u , the ODE $\dot{v} = -f(u, v)$ is bistable because it has two stable equilibria $h_1^{-1}(u)$ and $h_2^{-1}(u)$, and one unstable equilibrium $-u$. The condition in which $\dot{u} = f(u, v)$ is monostable for each fixed v is opposite to a condition in [15, 16] in which $\dot{u} = f(u, v)$ is bistable for each fixed v , which is used for a standard argument concerning the traveling waves and transition layers of reaction-diffusion systems (cf. [20] and the references therein). In contrast, we are concerned with unimodal patterns of (1.1) with (1.2), which do not need such an argument.

3 Spatiotemporal patterns of unperturbed system

In this section, we investigate spatiotemporal patterns of the unperturbed system (1.1) with (1.2), which is useful for understanding spontaneous cell polarization without extracellular signals. In particular, we numerically show limit cycles that exhibit an alternating repetition of unimodal and spatially homogeneous patterns. These limit cycles can be interpreted as cell polarity oscillations.

3.1 Concrete expression of localized unimodal stationary pattern

We give a concrete expression of a localized unimodal stationary pattern of (1.1) with (1.2) for sufficiently large K .

We consider stationary solutions of (1.1), i.e.,

$$\begin{cases} d_1 u_{xx} + f(u, v) = 0 \\ d_2 v_{xx} - f(u, v) = 0, \end{cases} \quad (3.1)$$

where $f(u, v)$ is given by (1.2). Applying a transformation of variables

$$p := u + v \quad \text{and} \quad q := \alpha u + v \quad (3.2)$$

to (3.1), we have

$$\begin{cases} q_{xx} = 0 \\ d_1 d_2 p_{xx} + (d_2 - d_1) a_1 p (pq - a_2) = 0. \end{cases} \quad (3.3)$$

Since q satisfies the periodic boundary condition, it follows from the first equation of (3.3) that $q(x) \equiv q_0$. Therefore, by the second equation of (3.3), we have

$$p_{xx} + c_1 p (p - c_2) = 0, \quad (3.4)$$

where

$$c_1 = \frac{(d_2 - d_1) a_1 q_0}{d_1 d_2} \quad \text{and} \quad c_2 = \frac{a_2}{q_0}.$$

On the other hand, a direct calculation shows that

$$p(x) = p_0 \operatorname{sech}^2(bx)$$

satisfies (3.4) for

$$p_0 = \frac{3a_2}{2q_0} \quad \text{and} \quad b = \frac{1}{2} \sqrt{\frac{(d_2 - d_1) a_1 a_2}{d_1 d_2}}. \quad (3.5)$$

Therefore, noting (3.2), we see that

$$u = \varphi_1(x) := \frac{1}{d_2 - d_1} \left(d_2 p_0 \operatorname{sech}^2(bx) - \frac{3a_2 d_2}{2p_0} \right) \quad (3.6)$$

and

$$v = \varphi_2(x) := \frac{1}{d_2 - d_1} \left(-d_1 p_0 \operatorname{sech}^2(bx) + \frac{3a_2 d_2}{2p_0} \right) \quad (3.7)$$

satisfy (3.1). Since $\operatorname{sech}(bx) = O(e^{-b|x|})$ as $|x| \rightarrow \infty$, it is easy to see that (1.1) has a stationary solution $(\bar{u}(x), \bar{v}(x))$ satisfying the periodic boundary condition at $x = \pm K/2$, where

$$\bar{u}(x) = \varphi_1(x) + O(e^{-bK}) \quad (3.8)$$

and

$$\bar{v}(x) = \varphi_2(x) + O(e^{-bK}) \quad (3.9)$$

as $K \rightarrow \infty$. We consider that $(\bar{u}(x), \bar{v}(x))$ is a localized unimodal stationary pattern as shown in Figure 2(b) when $p_0 > 0$ and K is sufficiently large. Moreover, we note that $(\bar{u}(x - c), \bar{v}(x - c))$ for some $c \in [-K/2, K/2]$ is also a stationary solution of (1.1) because of the periodic boundary condition.

It follows from (3.8) and (3.9) that

$$\bar{u}(x) + \bar{v}(x) = p_0 \operatorname{sech}^2(bx) + O(e^{-bK}) \quad (3.10)$$

and

$$\alpha \bar{u}(x) + \bar{v}(x) = q_0 + O(e^{-bK}). \quad (3.11)$$

Since

$$\int_I \operatorname{sech}^2(bx) dx = \int_{-\infty}^{\infty} \operatorname{sech}^2(bx) dx + O(e^{-bK}) = \frac{2}{b} + O(e^{-bK}),$$

integrating (3.10) over $I = (-K/2, K/2)$, we have

$$p_0 = \frac{b}{2} \int_I (\bar{u}(x) + \bar{v}(x)) dx + O(K e^{-bK}) \quad (3.12)$$

as $K \rightarrow \infty$. This implies that the amplitude of the localized stationary pattern given by (3.8) and (3.9) can be explicitly determined by the total mass of components.

3.2 Formation of localized unimodal pattern

We numerically investigate the formation process of a localized unimodal pattern of (1.1) with (1.2). Our numerical simulations show that a solution starting from a spatially homogeneous initial state with a small disturbance converges to $(\bar{u}(x - c), \bar{v}(x - c))$ for some $c \in [-K/2, K/2)$ under certain conditions, where \bar{u} and \bar{v} are given by (3.8) and (3.9), respectively.

Noting the mass conservation property (1.6) and (3.12), we see that the amplitude of the localized stationary pattern given by (3.8) and (3.9) is determined by

$$p_0 = \frac{bK}{2}\xi + O(Ke^{-bK}) \quad (3.13)$$

for sufficiently large K , where

$$\xi = \frac{1}{K} \int_I (u(x, 0) + v(x, 0)) dx \quad (3.14)$$

can be considered as a parameter. For each fixed ξ , we numerically solve (1.1) for various values of d_1 under the parameter values

$$a_1 = 0.5, \quad a_2 = 2.2, \quad d_2 = 1.0. \quad (3.15)$$

We choose $K = 10.0$ in such a way that $(\varphi_1(x), \varphi_2(x))$ can be numerically regarded as a stationary solution satisfying the periodic boundary condition. The initial value $(u(x, 0), v(x, 0))$ is given by $(\xi/2, \xi/2)$ with a small random perturbation, which means that the initial states of u and v are almost the same and spatially homogeneous. Notice that these parameter values are the same as those in [23].

We use a numerical scheme in [11] based on the pseudospectral method; we obtain numerical solutions of (1.1) on $0 \leq x \leq K$, which can be regarded as those on $-K/2 \leq x \leq K/2$ under the periodic boundary condition. The dynamics of numerical solutions consists of two stages. In the first stage, it is governed by the ODE (2.3), and the solutions approach a stable equilibrium of the ODE (2.1), which is given by (2.4). Figure 2 shows the second stage where the solutions converge to the localized unimodal stationary pattern given by $(\bar{u}(x-c), \bar{v}(x-c))$ for some $c \in [-K/2, K/2)$ under the parameter values (3.15) for $d_1 = 0.1$ when $\xi = 2.0$. Notice that we cannot predict the value of c , the position of the peak of the localized unimodal stationary pattern, because of a small random perturbation to the initial value of a solution. The formation process of a localized unimodal stationary pattern as presented in Figure 2 can be interpreted as cell polarization [23].

Our simulations show that when $\xi = 2.0$, numerical solutions converge to a (localized) unimodal stationary pattern for $d_1 \lesssim 0.73$, where the accuracy of approximation for the (localized) unimodal pattern by $(\bar{u}(x-c), \bar{v}(x-c))$ becomes lower as d_1 increases. We can obtain similar results when $\xi \gtrsim 0.68$.

Remark 3.1 Numerical simulations for the large values of ξ are delicate task. In fact, when $\xi = 2.0$, the numerical result shown in Figure 2 can be obtained if we adopt the time step as $\Delta t = 0.02$. In contrast, when $\xi = 6.0$, we can obtain a correct numerical result as shown in Figure 2 if $\Delta t = 0.01$.

Remark 3.2 We perform numerical simulations for $\xi > 0$. When $\xi < 0$, noting $p_0 < 0$ by (3.13), it follows from (3.6) and (3.7) that $(\bar{u}(x-c), \bar{v}(x-c))$ represents a localized anti-unimodal stationary pattern where the u -component has a single hole. We can observe the dynamics of anti-unimodal patterns, which is similar to that of unimodal patterns as shown in Figures 2 and 3. We do not consider the case $\xi = 0$ that numerical solutions do not move.

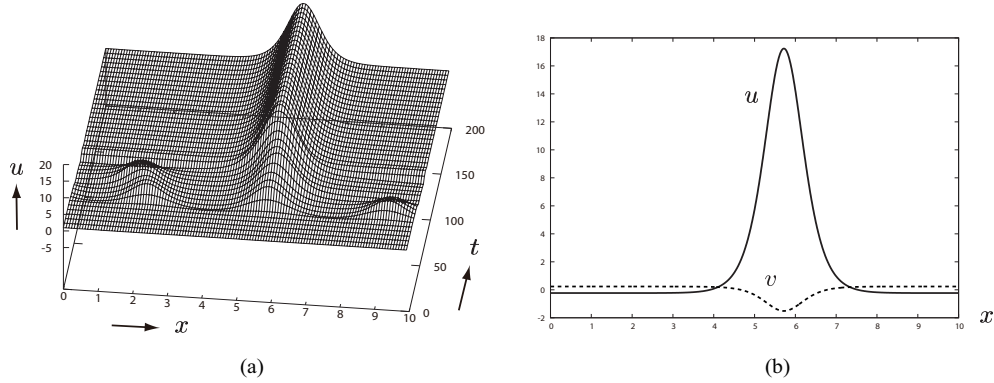


Figure 2: Formation of a localized unimodal stationary pattern for $d_1 = 0.1$ when $\xi = 2.0$. The initial value $(u(x, 0), v(x, 0))$ is given by $(\xi/2, \xi/2)$ with a small random perturbation. (a) The dynamics of u -component. The values of $u(x, t)$ on $0 \leq x \leq 10$ and $0 \leq t \leq 200$ are represented by a 3D graph. The profile of $v(x, t)$ is omitted here because the amplitude and spatial variation of $v(x, t)$ for each t are relatively small as compared to those of $u(x, t)$. (b) The profiles of $u(x, t)$ and $v(x, t)$ for $t = 200$, which can be regarded as the localized unimodal stationary pattern given by $(\bar{u}(x - c), \bar{v}(x - c))$ for some $c \in [-K/2, K/2)$. The rigid and dashed lines represent u - and v -components, respectively. The numerical solutions on $0 \leq x \leq 10$ presented in this figure can be regarded as those on $-5 \leq x \leq 5$ under the periodic boundary condition. It should be noted that we cannot predict the value of c , the position of the peak of the localized unimodal pattern in u -component, because of a small random perturbation to the initial value of a solution.

3.3 Spatiotemporal oscillatory patterns

We cannot observe that numerical solutions converge to the localized unimodal stationary pattern given by $(\bar{u}(x - c), \bar{v}(x - c))$ under certain conditions. In fact, when $\xi \lesssim 0.66$, our simulations show that the localized unimodal stationary pattern becomes unstable and spatiotemporal oscillatory patterns appear for some values of d_1 under the parameter values (3.15).

In the same way as the previous subsection, we perform numerical simulations for $d_1 = 0.1, 0.25, 0.4$ and $d_1 = 0.8$ when $\xi = 0.6$. Figure 3 shows that various spatiotemporal patterns appear in the second stage of the dynamics of numerical solutions when $\xi = 0.6$. Figure 3 (a) shows a localized unimodal stationary pattern, which can be interpreted as the persistent maintenance of cell polarity. Figures 3 (b) and (c) show stable limit cycles with large amplitude, which exhibit an alternating repetition of unimodal and spatially homogeneous patterns. Figure 3 (c) shows that the periodically appearing localized unimodal patterns take their maximum at $x = x_0$ for some $x_0 \in [-K/2, K/2]$ when $d_1 = 0.4$. In contrast, Figure 3 (b) shows that the periodically appearing localized unimodal patterns take their maximum at $x = x_1$ or $x = x_2$ alternatively for some $x_1 \in [-K/2, K/2]$ and $x_2 \in [-K/2, K/2]$ with $|x_2 - x_1| \approx K/2$ when $d_1 = 0.25$. These limit cycles in Figures 3 (b) and (c) can be interpreted as cell polarity oscillations. The limit cycle in Figure 3 (c) represents cell polarity oscillations with no reversal of polarity. In contrast, noting that x_2 is antipodal to x_1 , the limit cycle in Figure 3 (b) represents cell polarity oscillations with the reversal of polarity. We cannot predict the position of the peak of each localized unimodal pattern in Figures 3 (a)–(c) because of a small random perturbation to the initial value of a solution. Figure 3 (d) shows a spatially homogeneous stationary pattern, which can be interpreted as nonpolarized cells.

Remark 3.3 In the case of melanoma cells [24, Figure 2], spatially homogeneous stationary patterns as in Figure 3 (d) may be considered as cells that randomly polarize into frequently changing directions.

Remark 3.4 Recalling the fact that the ODE dynamics of (2.1) with (2.2) does not qualitatively change when we vary $\alpha \in (0, 1)$, we can obtain similar spatiotemporal patterns as shown in Figure 3 when we choose appropriate values of d_1 in (1.1) with (1.2) for fixed α . The reason why we impose the condition (1.3) is that we can perform concrete calculations as seen in Subsections 3.1 and 5.1. Moreover, our numerical computations of (1.1) with (1.2) by using the pseudospectral method are unlikely to cause numerical instabilities under the condition (1.3) as compared to the case without (1.3).

4 Numerical bifurcation analysis

In this section, we numerically demonstrate that the bifurcation diagram of (1.1) with (1.2) contains a structure that generates spatiotemporal patterns as presented in the last section. By using AUTO [2], a software package used for studying the bifurcation structure of ODE systems, we investigate the bifurcation diagram of an ODE system, which is obtained by the finite Fourier series approximation for (1.1) with (1.2) in the same way as [9]. We investigate the bifurcation diagram of the ODE system with respect to d_1 for some fixed values of ξ under the parameter values $a_1 = 0.5$, $a_2 = 2.2$ and $d_2 = 1.0$ by (3.15) and the interval length $K = 10.0$.

Figure 4 shows the bifurcation diagram with respect to d_1 for $\xi = 1.0$, where d_1 decreases from $d_1 = 0.8$. The primary branch starting from $d_1 = 0.8$

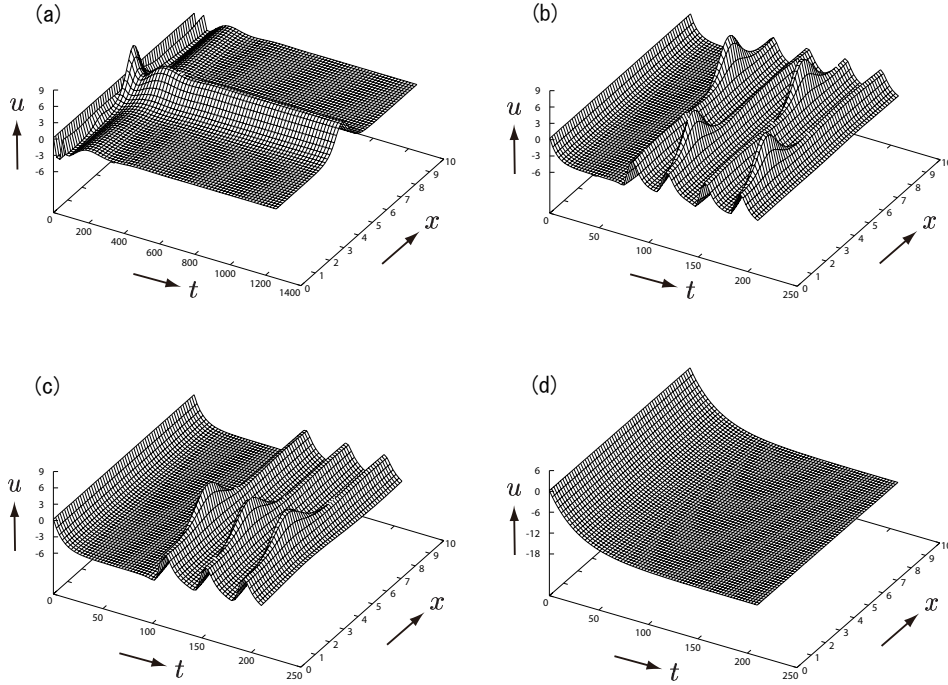


Figure 3: Spatiotemporal patterns appear in the second stage of the dynamics of numerical solutions for some values of d_1 when $\xi = 0.6$. The initial value is given by $(\xi/2, \xi/2)$ with a small random perturbation. The values of $u(x, t)$ on $(x, t) \in [0, 10] \times [0, 1400]$ or $(x, t) \in [0, 10] \times [0, 250]$ are represented by a 3D graph. The profile of $v(x, t)$ is omitted here because the amplitude and spatial variation of $v(x, t)$ for each t are relatively small as compared to those of $u(x, t)$. The numerical solution on $0 \leq x \leq 10$ presented in this figure can be regarded as that on $-5 \leq x \leq 5$ under the periodic boundary condition. (a) $d_1 = 0.1$, A localized unimodal stationary pattern; (b) $d_1 = 0.25$, An oscillatory pattern that exhibits an alternating repetition of spatially homogeneous patterns and localized unimodal patterns with two different positions of their peak. The distance between two peak positions is (almost) $K/2 = 5.0$. (c) $d_1 = 0.4$, An oscillatory pattern that exhibits an alternating repetition of spatially homogeneous patterns and localized unimodal patterns with unique peak positions. It should be noted that we cannot predict the position of the peak of each localized unimodal pattern in (a)–(c) because of a small random perturbation to the initial value of a solution. (d) $d_1 = 0.8$, A spatially homogeneous stationary pattern.

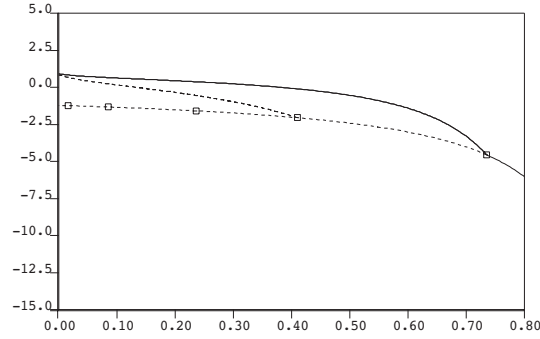


Figure 4: Bifurcation diagram with respect to d_1 for $\xi = 1.0$, where d_1 decreases from $d_1 = 0.8$. The horizontal and vertical axes indicate d_1 and the size of the u -component of solutions represented by $\frac{1}{K} \int_I u(x) dx$, respectively. The solid line indicates stable solutions, whereas the dashed line indicates unstable ones. The white square indicates the pitchfork bifurcation point. Unstable branches bifurcating from unstable branches for $d_1 \leq 0.30$ are omitted. Notice that the two branches bifurcating from a pitchfork bifurcation point are piled up and are displayed in this bifurcation diagram. The primary branch starting from $d_1 = 0.8$ represents a family of spatially homogeneous equilibria (4.1), which correspond to spatially homogeneous stationary patterns as shown in Figure 3(d). The secondary branch bifurcating from the primary branch via the supercritical pitchfork bifurcation at $d_1 \approx 0.74$ represents a family of (localized) unimodal stationary patterns as shown in Figure 3(a).

represents a family of spatially homogeneous equilibria

$$(u(x), v(x)) = \left(\frac{\xi^2 - a_2}{(1 - \alpha)\xi}, \frac{a_2 - \alpha\xi^2}{(1 - \alpha)\xi} \right) \quad (4.1)$$

with $\alpha = d_1/d_2$, which is given by (2.4). By using a standard linear stability analysis, we can easily verify that these equilibria are stable for $d_1 > d_1^c$ whereas unstable for $0 < d_1 < d_1^c$, where d_1^c is given by

$$d_1^c = \frac{a_1 a_2 d_2 K^2}{4\pi^2 + a_1 a_2 K^2}.$$

It should be noted that d_1^c is independent of ξ . When $d_1 = 0.8$, we have $d_1^c \approx 0.74$, which gives a supercritical pitchfork bifurcation point detected by AUTO in Figure 4. We should consider that this bifurcation is due to a diffusion-driven instability but not a well-known Turing instability. In fact, d_1 , the diffusion coefficient of u , is also included in the nonlinear term $f(u, v)$ by $\alpha = d_1/d_2$.

Remark 4.1 When we consider (1.1) with (1.2) for fixed α , we can similarly verify that a pitchfork bifurcation point where the stability of the equilibria (4.1) changes is given by

$$\tilde{d}_1^c = \frac{a_1 d_2 (\alpha \xi^2 + a_2) K^2}{4\pi^2 + (a_1 \xi^2 + a_1 a_2) K^2}.$$

In the strict sense, this bifurcation is not due to a Turing instability. In fact, as seen in Section 2, the equilibria (4.1) are stable in the ODE (2.1) obtained from (1.1) by dropping the diffusion terms. However, the linearized operator of the right hand side of (2.1) at (4.1) has zero eigenvalue, which implies that a well-known condition for Turing instability is not satisfied (cf. [18]). Therefore, the bifurcation in this case is sometimes called a Turing-like bifurcation [6].

The secondary branch bifurcates from the primary branch via the supercritical pitchfork bifurcation at $d_1 \approx 0.74$ as d_1 decreases. This stable branch represents a family of (localized) unimodal stationary patterns as shown in Figure 3(a). The bifurcation diagram presented in Figure 4 suggests that (1.1) with (1.2) has no limit cycles as shown in Figures 3(b) and (c). This type of bifurcation diagram can be obtained for $\xi \gtrsim 0.67$.

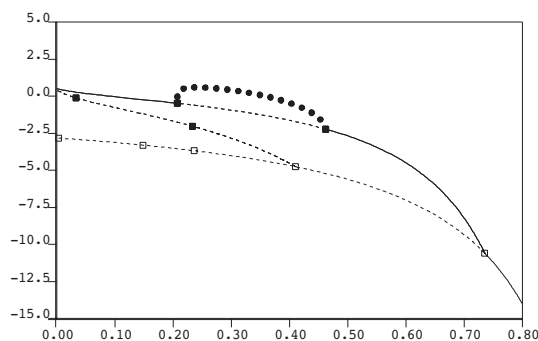


Figure 5: Bifurcation diagram with respect to d_1 for $\xi = 0.64$, where d_1 decreases from $d_1 = 0.8$. This bifurcation diagram is presented in the same way as that in Figure 4. The horizontal and vertical axes indicate d_1 and the size of the u -component of solutions represented by $\frac{1}{K} \max_{t>0} \int_I u(x, t) dx$, respectively. The white and black squares indicate the pitchfork and Hopf bifurcation points, respectively. The curve represented by a family of the black circles \bullet indicates the stable branch of periodic solutions. The primary branch starting from $d_1 = 0.8$ represents a family of spatially homogeneous equilibria (4.1), which correspond to spatially homogeneous stationary patterns as shown in Figure 3(d). The secondary branch bifurcating from the primary branch via the supercritical pitchfork bifurcation at $d_1 \approx 0.74$ represents a family of (localized) unimodal stationary patterns as shown in Figure 3(a). The third branch (indicated by \bullet) bifurcating from the second branch via the Hopf bifurcations at $d_1 \approx 0.46$ and $d_1 \approx 0.21$ represents a family of limit cycles as shown in Figure 3(c).

Figure 5 shows the bifurcation diagram for $\xi = 0.64$. As seen in Figure 4, the secondary branch consisting of (localized) unimodal stationary patterns

bifurcates from the primary branch consisting of spatially homogeneous equilibria via a supercritical pitchfork bifurcation at $d_1 \approx 0.74$ as d_1 decreases. However, (localized) unimodal stationary patterns on the second branch are unstable for $0.21 \lesssim d_1 \lesssim 0.46$. In fact, the third branch consisting of stable limit cycles as shown in Figure 3(c) bifurcates from the secondary branch via Hopf bifurcations at $d_1 \approx 0.46$ and $d_1 \approx 0.21$. In this case, we cannot observe limit cycles as shown in Figure 3(b). This type of bifurcation diagram can be obtained for $0.61 \lesssim \xi \lesssim 0.66$.

Figure 6 shows the bifurcation diagram for $\xi = 0.60$. As seen in Figure 5, the third branch consisting of limit cycles as shown in Figure 3(c) bifurcates from the second branch consisting of (localized) unimodal stationary patterns via Hopf bifurcations at $d_1 \approx 0.53$ and $d_1 \approx 0.14$. However, the third branch has unstable limit cycles for $0.13 \lesssim d_1 \lesssim 0.14$ and $0.18 \lesssim d_1 \lesssim 0.31$. We can observe limit cycles as shown in Figure 3(b) for $0.18 \lesssim d_1 \lesssim 0.31$, and expect that the fourth branch consisting of these limit cycles bifurcates from the third branch at $d_1 \approx 0.18$ and $d_1 \approx 0.31$ via period doubling bifurcations. In fact, AUTO detects a Floquet multiplier passing the unit circle $|\lambda| = 1$ through $\lambda = -1$ around $d_1 \approx 0.18$ and $d_1 \approx 0.31$. At present, it is technically difficult to trace this fourth branch by using AUTO. We can obtain similar bifurcation diagram as shown in Figure 6 for $\xi \lesssim 0.60$.

We can obtain bifurcation structures similar to those as described above near the specific parameter values (3.15). Figure 7 shows that the bifurcation diagram with respect to d_1 for $\xi = 0.60$ does not qualitatively change when we vary one of the values a_1 , a_2 , and d_2 near the specific values. Similarly, we can obtain the same results concerning the bifurcation diagrams with respect to d_1 for other values of ξ . Therefore, we conclude that the bifurcation structures presented in this section are structurally stable.

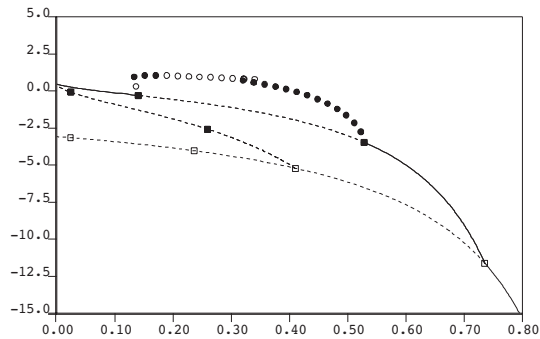


Figure 6: Bifurcation diagram with respect to d_1 for $\xi = 0.60$, where d_1 decreases from $d_1 = 0.8$. This bifurcation diagram is presented in the same way as that in Figure 5. The curve represented by a family of the black circles \bullet indicates the stable branch of periodic solutions, whereas that of the white circles \circ indicates the unstable one. The primary branch starting from $d_1 = 0.8$ represents a family of spatially homogeneous equilibria (4.1), which correspond to spatially homogeneous stationary patterns as shown in Figure 3(d). The secondary branch bifurcating from the primary branch via the supercritical pitchfork bifurcation at $d_1 \approx 0.74$ represents a family of (localized) unimodal stationary patterns as shown in Figure 3(a). The third branch (indicated by \bullet and \circ) bifurcating from the second branch via the Hopf bifurcations at $d_1 \approx 0.53$ and $d_1 \approx 0.14$ represents a family of limit cycles as shown in Figure 3(c). At present, we cannot trace the fourth branch bifurcating from the third branch via the period doubling bifurcations at $d_1 \approx 0.31$ and $d_1 \approx 0.18$. This branch that is not displayed here corresponds to a family of limit cycles as shown in Figure 3(b).

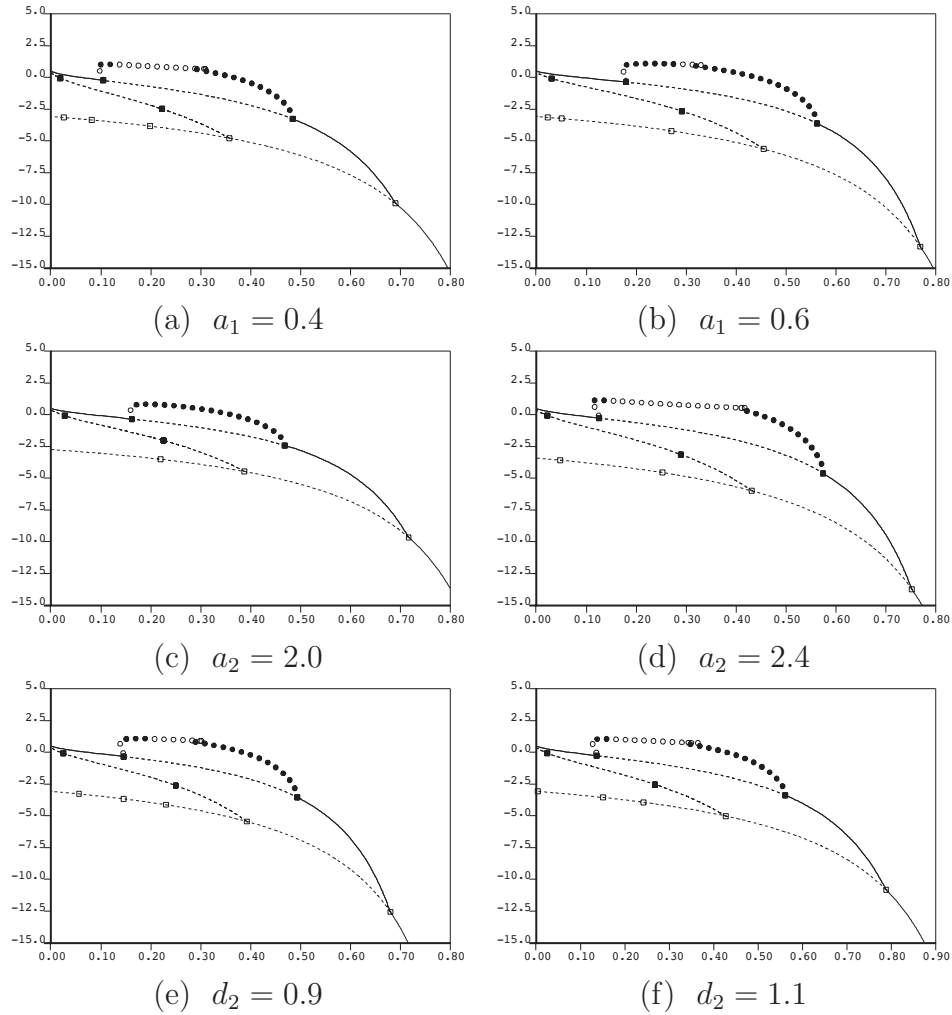


Figure 7: Bifurcation diagrams with respect to d_1 for $\xi = 0.60$ and the various values of a_1 , a_2 and d_2 . These bifurcation diagrams are presented in the same way as that in Figure 6. The parameter values except for the indicated value at the bottom of each figure are the same as those used in the bifurcation diagram presented in Figure 6, where $a_1 = 0.5$, $a_2 = 2.2$ and $d_2 = 1.0$ by (3.15). The bifurcation diagrams in (a) and (b) show that the bifurcation diagram in Figure 6 does not qualitatively change when we vary the value of a_1 near $a_1 = 0.5$. The bifurcation diagrams in (c) and (d) show that it does not qualitatively change when we vary the value of a_2 near $a_2 = 2.2$. The bifurcation diagrams in (e) and (f) show that it does not qualitatively change when we vary the value of d_2 near $d_2 = 1.0$.

5 Dynamics of spatiotemporal patterns of perturbed system

In this section, we investigate the dynamics of spatiotemporal patterns in the perturbed system (1.4) with (1.2) and (1.5). Our results are useful for understanding the effects of extracellular signals on cell polarization.

5.1 Motion of localized unimodal pattern

In the same way as Subsection 3.2, we find that a solution of (1.4) starting from a spatially homogeneous initial state with a small disturbance quickly and temporally approaches $(\bar{u}(x - c), \bar{v}(x - c))$ for some $c \in [-K/2, K/2]$ under certain conditions, where \bar{u} and \bar{v} are given by (3.8) and (3.9), respectively. Then, the solution translationally moves to the maximum point of $a_E(x)$, as shown in Figure 8. We derive the equation of motion for this translational movement according to [10]. In this subsection, to avoid confusion, we rewrite (1.1) and (1.4) as

$$\begin{cases} \dot{u} &= d_1 u_{xx} - f(u, v) \\ \dot{v} &= d_2 v_{xx} + f(u, v) \end{cases} \quad (5.1)$$

and

$$\begin{cases} \dot{u} &= d_1 u_{xx} - \{f(u, v) - \varepsilon g(x, u, v)\} \\ \dot{v} &= d_2 v_{xx} + \{f(u, v) - \varepsilon g(x, u, v)\}, \end{cases} \quad (5.2)$$

respectively, and (1.2) as

$$f(u, v) = -a_1(u + v)\{(\alpha u + v)(u + v) - a_2\}. \quad (5.3)$$

Moreover, to obtain a concrete and exact expression of the equation of motion, we consider that

$$g(x, u, v) = a_1(u + v)a_E(x), \quad (5.4)$$

where

$$a_E(x) = A \cos(2\pi x/K) \quad (5.5)$$

takes its maximum at $x = 0$. In this subsection, we carry our argument based on [10] by using (5.1)–(5.5).

We consider a solution that is well approximated by $S(x - \ell(t))$, where

$$S(x) := (\bar{u}(x), \bar{v}(x)) = (\varphi_1(x), \varphi_2(x)) + O(e^{-bK}), \quad (5.6)$$

and $\varphi_1(x)$ and $\varphi_2(x)$ are given by (3.6) and (3.7), respectively. Hereafter, we derive the equation for $\ell(t)$ by applying an argument in [10].

Remark 5.1 The theory of [10] was built on a mathematical assumption [10, Assumption 3.4], which guarantees that solutions stay in a small neighborhood of a manifold $M = \{S(x - \ell) \mid \ell \in \mathbf{R}\}$. Although such an assumption is indispensable to build a rigorous theory (cf. [5]), it is technically difficult to check it in many practical problems. Here, we formally apply an argument in [10] to our problem without checking the mathematical assumption.

First, we consider conditions that determine the sign of $\langle S_z, \Phi^* \rangle$ to be defined by (5.12). It follows from (5.6) that

$$S_x(x) = w(x)(d_2, -d_1),$$

where

$$w(x) = -\frac{2bp_0}{d_2 - d_1} \operatorname{sech}^2(bx) \tanh(bx) + O(e^{-bK}) \quad (5.7)$$

with

$$b = \frac{1}{2} \sqrt{\frac{(d_2 - d_1)a_1 a_2}{d_1 d_2}} \quad \text{and} \quad p_0 = \frac{bK}{2} \xi + O(K e^{-bK}) \quad (5.8)$$

by (3.5) and (3.13). Therefore, we see that $w(x) < 0$ for $x > 0$ as mentioned in [10, Lemma 3.2].

Since $f_v(u, v) = -2a_1(u + v)(\alpha u + v) - a_1(u + v)^2 + a_1a_2$ by (5.3), noting (3.10), (3.11) and $p_0q_0 = 3a_2/2$ by (3.5), we have

$$\begin{aligned} h_2(x) &:= -\frac{f_v(\bar{u}(x), \bar{v}(x))w(x)}{d_2} \\ &= \frac{2bp_0}{d_2(d_2 - d_1)} \operatorname{sech}^2(bx) \tanh(bx) F(x) + O(Ke^{-bK}) \end{aligned}$$

where $F(x) := -3a_1a_2 \operatorname{sech}^2(bx) - a_1p_0^2 \operatorname{sech}^4(bx) + a_1a_2$. Let $t = \operatorname{sech}^2(bx)$. Then, we have $F(x) = g(t)$, where

$$g(t) := -3a_1a_2t - a_1p_0^2t^2 + a_1a_2.$$

We see that $F(x)$ is monotone increasing in x for $x > 0$ because $t = \operatorname{sech}^2(bx)$ is monotone decreasing in x for $x > 0$ and $g(t)$ is monotone decreasing in t for $t > 0$. Moreover, we have $F(0) = g(1) = -2a_1a_2 - a_1p_0^2 < 0$ and $F(K/2) = g(0) + O(e^{-bK}) = a_1a_2 + O(e^{-bK}) > 0$. Therefore, there exists $\beta \in (0, K/2)$ such that $h_2(x) < 0$ for $0 < x < \beta$ and $h_2(x) > 0$ for $\beta < x < K/2$. Furthermore, noting (5.8), a direct calculation with the aid of Mathematica shows

$$\begin{aligned} \int_0^{K/2} x h_2(x) dx &= \frac{2ba_1p_0}{d_2(d_2 - d_1)} \left\{ -3a_2 \int_0^\infty x \operatorname{sech}^4(bx) \tanh(bx) dx \right. \\ &\quad \left. - p_0^2 \int_0^\infty x \operatorname{sech}^6(bx) \tanh(bx) dx + a_2 \int_0^\infty x \operatorname{sech}^2(bx) \tanh(bx) dx \right\} \\ &\quad + O(Ke^{-bK}) \\ &= \frac{2ba_1p_0}{d_2(d_2 - d_1)} \left\{ -3a_2 \cdot \frac{1}{6b^2} - p_0^2 \cdot \frac{4}{45b^2} + a_2 \cdot \frac{1}{2b^2} \right\} + O(Ke^{-bK}) \\ &= -\frac{8a_1p_0^3}{45(d_2 - d_1)d_2b} + O(Ke^{-bK}) = -\frac{4a_1p_0^2K\xi}{45(d_2 - d_1)d_2} + O(Ke^{-bK}). \end{aligned}$$

Therefore,

$$\int_0^{K/2} x h_2(x) dx < 0$$

holds if

$$\xi = \frac{1}{K} \int_I (u(x, 0) + v(x, 0)) dx > 0.$$

Hence, the condition (ii) of [10, Proposition 3.6] holds. Thus, we see that $\varphi_2^*(x) > 0$ for $0 < x < K/2$, where φ_2^* is an odd periodic function with the period K , which satisfies $(\varphi_2^*)'' = h_2$, $\varphi_2^*(0) = \varphi_2^*(K/2) = 0$, and

$$\frac{d\varphi_2^*}{dx}(K/2) = \frac{2}{K} \int_0^{K/2} x h_2(x) dx. \quad (5.9)$$

Next, we derive the equation for $\ell(t)$. It follows from [10, Equation (4.3)] that

$$\frac{d\ell}{dt} = -\varepsilon \frac{J(\ell)}{\langle S_z, \Phi^* \rangle} + O(\varepsilon^2), \quad (5.10)$$

where

$$J(\ell) := - \int_0^{K/2} a_1(\bar{u}(z) + \bar{v}(z)) w(z) \{a_E(z + \ell) - a_E(z - \ell)\} dz \quad (5.11)$$

and

$$\langle S_z, \Phi^* \rangle := -2d_2 \int_0^{K/2} w^2(z) dz + 2(d_2 - d_1) \int_0^{K/2} w(z) \varphi_2^*(z) dz. \quad (5.12)$$

The calculations of the right hand sides of (5.11) and (5.12) are rather lengthy, and found in the appendix. As a result, noting the second equation of (5.8), it follows from (5.10) that

$$\frac{d\ell}{dt} = -\varepsilon \left(C \sin\left(\frac{2\pi\ell}{K}\right) + O(Ke^{-bK}) \right) + O(\varepsilon^2), \quad (5.13)$$

where C is given by

$$C = \frac{5a_1 d_2 \pi^3 A(b^2 K^2 + \pi^2) \operatorname{cosech}\left(\frac{\pi^2}{bK}\right)}{b^3 K^4 \left\{ \frac{4b^2 d_2^2}{d_2 - d_1} + a_1 a_2 + \frac{2a_1 b K \xi^2}{21} (3bK - 7) \right\}}$$

with the first equation of (5.8). For example, the value of C is given by $C \approx 6.35 \times 10^{-3}$ under the same condition in the simulation by [23], i.e., $K = 10.0$, $\xi = 2.0$, $d_1 = 0.1$, $A = 1.1$ and the parameter values (3.15).

We now examine the validity of (5.13) from a viewpoint of numerical simulations. In a similar manner to the previous section, we numerically solve (5.2) with $a_E(x) = A \cos(\frac{2\pi}{K}(x - \frac{K}{2}))$ on $0 \leq x \leq K$ under the periodic boundary condition. In this case, neglecting error terms, (5.13) is replaced by

$$\frac{d\ell}{dt} = -\varepsilon C \sin\left(\frac{2\pi}{K}\left(\ell - \frac{K}{2}\right)\right). \quad (5.14)$$

Figure 8 shows that a localized unimodal pattern moves to the maximal point of $a_E(x)$ following the equation of motion given by (5.14). Here, the values of parameters are given by (3.15), and $K = 10.0$, $\xi = 2.0$, $d_1 = 0.1$, $A = 1.1$ and $\varepsilon = 0.1$. The initial value is given by $(\bar{u}(x - c), \bar{v}(x - c))$ with $c = 1.6$, where \bar{u} and \bar{v} are given by (3.8) and (3.9), respectively. We note that these results are valid for $0 < \varepsilon \lesssim 0.1$. This suggests that the translational movement of cell polarity can be controlled by sufficiently weak extracellular signals.

Remark 5.2 [23] studied (5.2) by setting $a_2 \rightarrow a_2 \left(1 + \frac{\varepsilon}{2} \sin(\frac{2\pi x}{K})\right)$ in (5.3), which is equivalent to $a_E(x) = A \cos(\frac{2\pi}{K}(x + \frac{K}{4}))$ with $A = a_2/2$. Their formal analysis for the translational movement of a localized unimodal pattern could not give a precise result because their analysis was done under the assumption in which the speed of the movement is constant.

5.2 Dynamics of spatiotemporal oscillatory patterns

The result in the last subsection suggests that the position of the peak of the final localized unimodal stationary pattern of (1.4) can be determined by the maximum point of $a_E(x)$. In this subsection, we investigate whether the perturbed system (1.4) has spatiotemporal oscillatory patterns as shown in

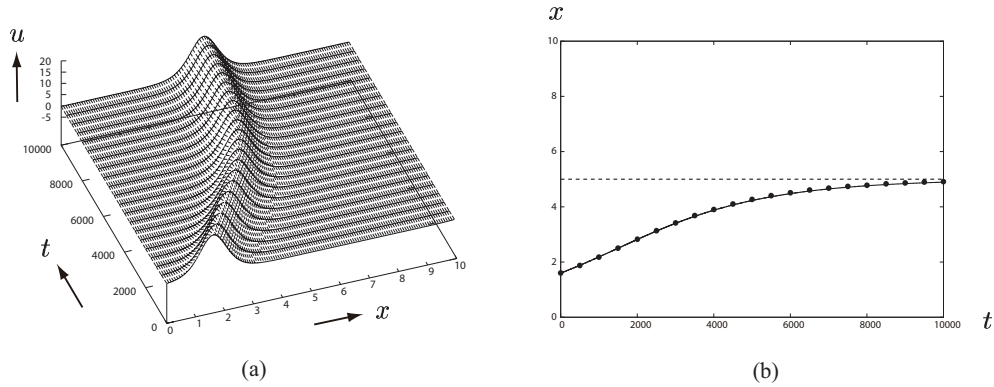


Figure 8: The motion of a localized unimodal pattern in the perturbed system (5.2). The initial value is given by $(\bar{u}(x - c), \bar{v}(x - c))$ with $c = 1.6$, where \bar{u} and \bar{v} are given by (3.8) and (3.9), respectively. (a) The dynamics of u -component. The values of $u(x, t)$ on $0 \leq x \leq 10$ and $0 \leq t \leq 10000$ are represented by a 3D graph. The profile of $v(x, t)$ is omitted here because the amplitude and spatial variation of $v(x, t)$ for each t are relatively small as compared to those of $u(x, t)$. (b) The comparison between the theory and numerical simulations. The rigid and dashed lines represent a solution of (5.14) with the initial value $\ell(0) = 1.6$ and its limit given by $\ell = 5.0$, respectively. The dots represent the maximal point of $u(x, t)$ for $t = 500n$ ($n \in \mathbf{Z}, 0 \leq n \leq 20$).

Figures 3 (b) and (c) under the same conditions imposed on the unperturbed system (1.1). In particular, we examine whether the position of the peak of such periodically appearing unimodal pattern can be determined by the maximum point of $a_E(x)$.

We consider (1.4) with (1.5) and $a_E(x) = A \cos(\frac{2\pi}{K}(x - \frac{K}{2}))$ on $0 \leq x \leq K$ under the periodic boundary condition. In the same way as Subsection 3.3, we numerically solve (1.4) for $d_1 = 0.1, 0.25, 0.4$ and $d_1 = 0.8$ when $\xi = 0.6$ under the parameter values (3.15) and $K = 10.0, A = 1.1$ and $\varepsilon = 0.1$.

Figure 9 shows that the perturbed system (1.4) exhibits similar spatiotemporal patterns as shown in Figure 3. In contrast to the case of the unperturbed system (1.1), the position of the peak of each localized unimodal pattern of the perturbed system (1.4) is determined by the maximum point of $a_E(x)$, i.e., it does not depend on a small random perturbation to the initial value of a solution. Moreover, we note that the stable limit cycles in the perturbed system (1.4) earlier appear and their period is shorter as compared to those in the unperturbed system (1.1).

When $d_1 = 0.4$, we can observe oscillatory spatiotemporal patterns as shown in Figure 9 (c) for $0 < \varepsilon \leq 0.1$. In contrast, when $d_1 = 0.25$, we cannot always observe oscillatory spatiotemporal patterns as shown in Figure 9 (b) for $0 < \varepsilon \leq 0.1$. More precisely, we can observe them for $0.015 \lesssim \varepsilon \leq 0.1$, i.e., the position of the peak of each localized unimodal pattern cannot be determined by the maximum point of $a_E(x)$ for $0 < \varepsilon \lesssim 0.014$. These results suggest that cell polarity oscillations can be controlled by sufficiently weak extracellular signals if the reversal of polarity does not occur.

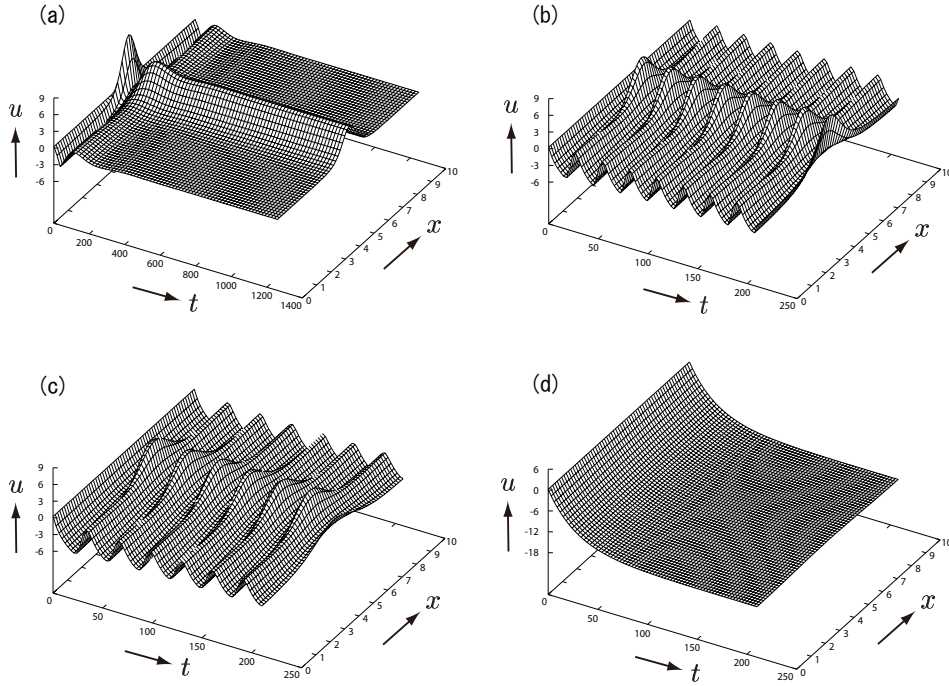


Figure 9: Spatiotemporal patterns appear for some values of d_1 when $\xi = 0.6$ and $\varepsilon = 0.1$. The initial value is given by $(\xi/2, \xi/2)$ with a small random perturbation. The 3D graphs are presented in the same way as those in Figure 3. (a) A localized unimodal stationary pattern for $d_1 = 0.1$; (b), (c) An oscillatory pattern that exhibits an alternating repetition of spatially homogeneous patterns and localized unimodal patterns with unique peak positions. The values of d_1 are given by $d_1 = 0.25$ and $d_1 = 0.4$, respectively. In contrast to the case of Figure 3, it should be noted that the position of the peak of each localized unimodal pattern in (a)–(c) is determined by the maximum point of $a_E(x)$ without depending on a small random perturbation to the initial value of a solution. (d) A spatially homogeneous stationary pattern for $d_1 = 0.8$.

6 Discussion

In this paper, we show that a reaction-diffusion system with bistable nonlinearity and mass conservation, proposed by [23], exhibits four different spatiotemporal patterns including two types of oscillatory patterns, which can be regarded as cell polarity oscillations with the reversal and non-reversal of polarity, respectively. The trigger causing these patterns is a diffusion-driven (Turing-like) instability. Moreover, we show that the periodic reversal is due to a period doubling bifurcation using a numerical bifurcation analysis. Furthermore, we investigate the effects of extracellular signals on cell polarity oscillations. Our results suggest that cell polarity oscillations can be controlled by sufficiently weak extracellular signals if the reversal of polarity does not occur.

To understand the biological implications of our results based on this model, we consider a cell (simplified and abstract model) with the following properties: (1) Cell polarity is controlled by chemical X . (2) The amount of X is conserved. (3) Chemical X has two states X_m and X_c . (4) The diffusion coefficient of X_c is faster than that of X_m . (5) The cell size K is conserved. Let $u = [X_m] - c_m$ and $v = [X_c] - c_c$, where $[X_m]$ and $[X_c]$ denote the concentrations of X_m and X_c , respectively, and c_m and c_c are the reference values of $[X_m]$ and $[X_c]$, respectively. Then, noting the conservation law (1.6), we have

$$\xi = \frac{1}{K} \int_0^K (u + v) dx = |X|/K - C,$$

where $|X|$ denotes the amount of X , and $C = c_m + c_c$ is a positive constant independent of $|X|$ and K . Recalling that we consider $\xi = |X|/K - C > 0$ as a parameter in our numerical simulations and bifurcation analysis, our results are then summarized as follows: (1) Cell polarity can be established

for the appropriate values of the diffusion coefficients of X_m and X_c . (2) Cell polarity oscillations can be observed for the appropriate values of the diffusion coefficients of X_m and X_c when ξ is relatively small. Assertion (1) can also be obtained from other reaction-diffusion models [6, 23]. In contrast, assertion (2) is a characteristic of our results based on the reaction-diffusion model (1.1) with (1.2). When $|X|$ is constant, we can regard K as a bifurcation parameter. Let us suppose a situation in which the parameter K increases whereas $|X|$ is constant, and consider that this situation corresponds to the stage (just) before cell division. We can then see that cell polarity oscillations can be observed (just) before cell division, which is consistent with our naive intuition (cf. [3]). Similarly, when K is constant, we can regard $|X|$ as a bifurcation parameter. We suppose a situation in which the parameter $|X|$ decreases whereas K is constant. We can then see that cell polarity oscillations occur when the amount of chemical X decreases. This implies that chemical X is indispensable for freezing cell polarity.

In simple terms, mathematical models for studying cell polarity oscillations are classified into two types, i.e., ODE models and reaction-diffusion models. In general, ODE models are based on concrete molecular species and networks, and explicitly or implicitly assume the existence of the front and back of a cell. Such models cannot represent cell polarity oscillations with the non-reversal of polarity, as observed in cells in a developing epithelial tissue [3]. In contrast, the reaction-diffusion model (1.1) with (1.2) can represent cell polarity oscillations with both the non-reversal and reversal of polarity. Moreover, we note that it does not assume a priori the existence of the front and back of a cell.

The Gierer-Meinhardt model [14] seems to be the first reaction-diffusion system in history, which can be used to study spatiotemporal patterns con-

sisting of (many) localized unimodal patterns. This model has been considered as a reference for studying cell polarity, and [14] noticed that oscillations are necessary for the reorientation of polarity. However, they did not give any concrete information concerning the oscillations. More than twenty years later, [13] proposed an ODE system consisting of many components (cells), which can represent cell polarity oscillations with the periodic reversal of polarity. Consequently, as shown in a review paper [7], reaction-diffusion models have been considered to be undesirable for representing the dynamic maintenance of cell polarity such as cell polarity oscillations. Our result suggests a counter-example for such a common view, i.e., (1.1) with (1.2) can be a simple reaction-diffusion model for studying cell polarity oscillations.

A reaction-diffusion model of the Rho GTPases (Rac, Cdc42, RhoA), which are key regulators for cell polarity, was also proposed by [23]. Moreover, [23] compared this model with reaction-diffusion models proposed by [19, 27], which are based on a phosphoinositide cycle that recruits and activates the Rho GTPases (Rac, Cdc42). Consequently, the dynamics of these models share common properties, which can be interpreted as follows: (1) the spontaneous formation of cell polarity, (2) the uniqueness of polarity determining the axis of a cell, (3) the polarized sensitivity wherein a polarized cell responds to a change in the extracellular signal gradient. Although these models based on the concrete molecular species and networks are considerably realistic, they consist of many components and have complicated nonlinear terms, and hence it is difficult to understand a mechanism for generating the dynamics with three properties. Therefore, [23] provided the concept of reaction-diffusion systems with mass conservation, which is given by (1.1). In fact, the realistic models include the structure of (1.1), and it was shown in [23] that (1.1) can exhibit dynamics with three properties for

appropriate nonlinear terms $f(u, v)$.

The reaction-diffusion system (1.1) with (1.2) is a phenomenological model, which may not explicitly correspond to concrete molecular species and networks. Therefore, at present, our results may not be applicable to practical biological problems. However, as was mentioned above, the reaction-diffusion system (1.1) with (1.2) can exhibit the dynamics observed in the realistic models proposed by [19, 23, 27]. Hence, it is important to explore a parameter region where these realistic models exhibit cell polarity oscillations. Once we find such a region, we can propose physical characteristics or parameters related to mechanisms for switching cell polarity, and can therefore compare our results with those in [28]. Moreover, we might propose experimentally testable hypotheses concerning cell polarity oscillations with the aid of biologists.

Since our results were obtained using a specific reaction-diffusion system with bistable nonlinearity and mass conservation, it is also important to investigate conditions in which general reaction-diffusion systems with bistable nonlinearity and mass conservation can generate cell polarity oscillations. This investigation will consist of three steps: (1) investigating conditions in which (1.1) with bistable nonlinearity has a localized unimodal stationary pattern, (2) investigating conditions in which the unimodal pattern becomes unstable through a Hopf bifurcation with respect to the ratio of the diffusion coefficients by a normal form analysis, as presented in [22], (3) investigating conditions in which oscillatory patterns bifurcating from the unimodal pattern undergo a period doubling bifurcation by a numerical bifurcation analysis, as presented herein. We expect that the generalization of nonlinear terms will provide a viewpoint for exploring biological phenomena, which can be studied by reaction-diffusion systems with bistable nonlinearity and mass

conservation.

Acknowledgments. The authors would like to express their appreciation to the referees for their useful suggestions and comments, which have improved the original manuscript. The first, second, and third authors were supported in part by the JSPS KAKENHI 16K05273, 17K14237, 19H01805, respectively.

Appendix The calculations of the right hand sides of (5.11) and (5.12)

Noting (3.10), (5.5), (5.7) and

$$\cos\left(\frac{2\pi(z+\ell)}{K}\right) - \cos\left(\frac{2\pi(z-\ell)}{K}\right) = -2\sin\left(\frac{2\pi z}{K}\right)\sin\left(\frac{2\pi\ell}{K}\right),$$

a direct calculation with the aid of Mathematica shows

$$\begin{aligned} J(\ell) &= -\int_0^{K/2} a_1(\bar{u}(z) + \bar{v}(z))w(z)\{a_E(z+\ell) - a_E(z-\ell)\}dz \\ &= -\frac{4a_1bp_0^2A}{d_2-d_1}\sin\left(\frac{2\pi\ell}{K}\right)\int_0^\infty \operatorname{sech}^4(bz)\tanh(bz)\sin\left(\frac{2\pi z}{K}\right)dz + O(Ke^{-bK}) \\ &= -\frac{4a_1bp_0^2A}{d_2-d_1} \cdot \frac{\pi^3(b^2K^2 + \pi^2)}{3b^5K^4} \cdot \operatorname{cosech}\left(\frac{\pi^2}{bK}\right)\sin\left(\frac{2\pi\ell}{K}\right) + O(Ke^{-bK}). \end{aligned}$$

Similarly, we have

$$\begin{aligned} \int_0^{K/2} w^2(z)dz &= \frac{4b^2p_0^2}{(d_2-d_1)^2}\int_0^\infty \operatorname{sech}^4(bz)\tanh^2(bz)dz + O(Ke^{-bK}) \\ &= \frac{8bp_0^2}{15(d_2-d_1)^2} + O(Ke^{-bK}). \end{aligned}$$

Since $(\operatorname{sech}^2(bx))' = -2b\operatorname{sech}^2(bx)\tanh(bx)$, $\tanh(bx)' = b\operatorname{sech}^2(bx)$, and $(\varphi_2^*)'' = h_2$, using (5.9), $\varphi_2^*(0) = \varphi_2^*(K/2) = 0$, and the integration by parts

twice, we have

$$\begin{aligned}
2(d_2 - d_1) \int_0^{K/2} w(z) \varphi_2^*(z) dz &= 2p_0 \int_0^{K/2} (\operatorname{sech}^2(bz))' \varphi_2^*(z) dz \\
&= -2p_0 \int_0^{K/2} \operatorname{sech}^2(bz) (\varphi_2^*(z))' dz = -\frac{2p_0}{b} \int_0^{K/2} (\tanh(bz))' (\varphi_2^*(z))' dz \\
&= -\frac{2p_0}{b} \left\{ \frac{d\varphi_2^*}{dx}(K/2) - \int_0^{K/2} \tanh(bz) (\varphi_2^*(z))'' dz \right\} \\
&= -\frac{2p_0}{b} \left\{ \frac{2}{K} \int_0^{K/2} x h_2(x) dx - \int_0^{K/2} \tanh(bz) h_2(z) dz \right\},
\end{aligned}$$

where we abbreviate error terms denoted by $O(Ke^{-bK})$. Moreover, a direct calculation with the aid of Mathematica shows

$$\begin{aligned}
\int_0^{K/2} \tanh(bz) h_2(z) dz &= -\frac{2a_1 b p_0}{d_2(d_2 - d_1)} \left\{ 3a_2 \int_0^\infty \operatorname{sech}^4(bz) \tanh^2(bz) dz \right. \\
&\quad \left. + p_0^2 \int_0^\infty \operatorname{sech}^6(bz) \tanh^2(bz) dx - a_2 \int_0^\infty \operatorname{sech}^2(bz) \tanh^2(bz) dz \right\} + O(Ke^{-bK}) \\
&= -\frac{2a_1 b p_0}{d_2(d_2 - d_1)} \left\{ 3a_2 \cdot \frac{2}{15b} + p_0^2 \cdot \frac{8}{105b} - a_2 \cdot \frac{1}{3b} \right\} + O(Ke^{-bK}) \\
&= -\frac{2a_1 p_0}{d_2(d_2 - d_1)} \left\{ \frac{a_2}{15} + \frac{8p_0^2}{105} \right\} + O(Ke^{-bK}).
\end{aligned}$$

Therefore, we have

$$\begin{aligned}
\langle S_z, \Phi^* \rangle &= -2d_2 \int_0^{K/2} w^2(z) dz + 2(d_2 - d_1) \int_0^{K/2} w(z) \varphi_2^*(z) dz \\
&= -\frac{4p_0^2}{15(d_2 - d_1)} \left\{ \frac{4bd_2}{d_2 - d_1} + \frac{a_1 a_2}{bd_2} + \frac{8a_1 p_0^2}{bd_2} \left(\frac{1}{7} - \frac{1}{3Kb} \right) \right\} + O(Ke^{-bK}) < 0.
\end{aligned}$$

References

- [1] J. L. Chern, Y. Morita, and T. T. Shieh, Asymptotic behavior of equilibrium states of reaction-diffusion systems with mass conservation, *J. Diff. Eqns.* **264** (2018), 550–574.
- [2] E. J. Doedel, B. E. Oldeman, A. R. Champneys, F. Dercole, T. Fairgrieve, Y. A. Kuznetsov, R. C. Paffenroth, B. Sandstede, X. Wang, C. Zhang, AUTO-07p: continuation and bifurcation software for ordinary differential equations (2012).
- [3] S. Doerr, K. Ragkousi, Cell polarity oscillations in mitotic epithelia, *Current Opinion in Genetics and Development*, **57** (2019), 47-53.
- [4] M. Guzzo, S. M. Murray, E. Martineau, S. Lhospice, G. Baronian, L. My, et al. A gated relaxation oscillator mediated by FrzX controls morphogenetic movements in *Myxococcus xanthus*, *Nature Microbiology*, **3** (2018), 948-959.
- [5] D. Henry, *Geometric Theory of Semilinear Parabolic Equations*, Lecture Note in Math. 840, Springer-Verlag, New York, 1981.
- [6] S. Ishihara, M. Otsuji, A. Mochizuki, Transient and steady state of mass-conserved reaction-diffusion systems, *Phys. Rev. E* **75** (2007), 015203.
- [7] A. Jilkine, L. Edelstein-Keshet, A comparison of mathematical models for polarization of single eukaryotic cells in response to guided cues, *PLoS Comput. Biol.*, **3** (2011), e1001121.
- [8] S. Jimbo, Y. Morita, Lyapunov function and spectrum comparison for a reaction-diffusion system with mass conservation, *J. Diff. Eqns* **255** (2013), 1657-1683.

- [9] M. Kuwamura and H. Izuhara, Diffusion-driven destabilization of spatially homogeneous limit cycles in reaction-diffusion systems, *Chaos*. **27** (2017), 033112.
- [10] M. Kuwamura, S.-S. Lee, S.-I. Ei, Dynamics of localized unimodal patterns in reaction-diffusion systems for cell polarization by extracellular signaling, *SIAM J. Appl. Math.* **78** (2018), 3238-3257.
- [11] M. Kuwamura, Y. Morita, Perturbations and dynamics of reaction-diffusion systems with mass conservation, *Phys. Rev. E* **92** (2015), 012908.
- [12] Y. Liu, W.-C. Lo, Analysis of spontaneous emergence of cell polarity with delayed negative feedback, *Math. Biosci. Eng.* **16** (2019), 1392-1413.
- [13] H. Meinhardt, Orientation of chemotactic cells and growth cones: models and mechanisms, *J. Cell Sci.* **112** (1999), 2867-2874.
- [14] H. Meinhardt, A. Gierer, Applications of a theory of biological pattern formation based on lateral inhibition, *J. Cell Sci.* **15** (1974), 321-346.
- [15] Y. Mori, A. Jilkine, L. Edelstein-Keshet, Wave-pinning and cell polarity from a bistable reaction-diffusion system, *Biophys. J.* **94** (2008), 3684-3697.
- [16] Y. Mori, A. Jilkine, L. Edelstein-Keshet, Asymptotic and bifurcation analysis of wave-pinning in a reaction-diffusion model for cell polarization, *SIAM J. Appl. Math* **71** (2011), 1401-1427.

- [17] Y. Morita, T. Ogawa, Stability and bifurcation of nonconstant solutions to a reaction-diffusion system with conservation of mass, *Nonlinearity* **23** (2010), 1387-1411.
- [18] Murray, J.D., *Mathematical Biology*, 2nd ed. Springer-Verlag, New York, 1989.
- [19] A. Narang, K. K. Subramanian, D. A. Lauffenburger, A Mathematical Model for Chemoattractant Gradient Sensing Based on Receptor-Regulated Membrane Phospholipid Signaling Dynamics, *Ann. of Biomedical Eng.* **29** (2001), 677-691.
- [20] Y. Nishiura, H. Fujii, Stability of singularly perturbed solutions to systems of reaction-diffusion equations, *SIAM J. Math. Anal.* **18** (1987), 1726-1770.
- [21] Okubo, A., Levin, S.A., *Diffusion and Ecological Problems*, 2nd ed. Springer-Verlag, New York, 2001
- [22] T. Okuda Sakamoto, Hopf bifurcation in a reaction-diffusion system with conservation of mass, *Nonlinearity* **26** (2013), 2027-2049.
- [23] M. Otsuji, S. Ishihara, C. Co, K. Kaibuchi, A. Mochizuki, S. Kuroda, A mass conserved reaction-diffusion system captures properties of cell polarity, *PLoS Comp. Biol.* **3** (2007), e108.
- [24] J. Parka, W. R. Holmes, S. H. Lee, H.-N. Kim, D.-H. Kim, M. K. Kwak, C. J. Wang, L. Edelstein-Keshet, A. Levchenko, Mechanochemical feedback underlies coexistence of qualitatively distinct cell polarity patterns within diverse cell populations, *Proc Natl Acad Sci U S A* **114** (2017), E5750-E5759.

- [25] O. Sliusarenko, J. Neu, D. R. Zusman, G. Oster, Accordion waves in *Myxococcus xanthus*, Proc Natl Acad Sci U S A **103** (2006), 1534-1539.
- [26] J. Smoller, Shock Waves and Reaction-Diffusion Equations, Springer-Verlag, New York, 1994.
- [27] K. K. Subramanian, A. Narang, A mechanistic model for eukaryotic gradient sensing: spontaneous and induced phosphoinositide polarization, J. Theo. Biol. **231** (2004), 49-67.
- [28] F. Tostevin, M. Wigbers, L. Sogaard-Andersen, U. Gerland, Four different mechanisms for switching cell polarity, PLoS Comp. Biol. **17** (2021), e1008587.